

Conv1D Energy-Aware Path Planner for Mobile Robots in Unstructured Environments

Marco Visca, Arthur Bouton, Roger Powell, Yang Gao and Saber Fallah

Abstract—Driving energy consumption plays a major role in the navigation of mobile robots in challenging environments, especially if they are left to operate unattended under limited on-board power. This paper reports on first results of an energy-aware path planner, which can provide estimates of the driving energy consumption and energy recovery of a robot traversing complex uneven terrains. Energy is estimated over trajectories making use of a self-supervised learning approach, in which the robot autonomously learns how to correlate perceived terrain point clouds to energy consumption and recovery. A novel feature of the method is the use of 1D convolutional neural network to analyse the terrain sequentially in the same temporal order as it would be experienced by the robot when moving. The performance of the proposed approach is assessed in simulation over several digital terrain models collected from real natural scenarios, and is compared with a heuristic inclination-based energy model. We show evidence of the benefit of our method to increase the overall prediction r^2 score by 66.8% and to reduce the driving energy consumption over planned paths by 5.5%.

I. INTRODUCTION

Autonomous path planning of mobile robots in unstructured environments is a crucial task in many sectors such as: rescue robots for disaster area, agriculture, nuclear plants, and space exploration. Among different factors, energy consumption can play a major role on the success and efficiency of robotic missions. For example, planetary exploration rovers are required to drive several kilometres to reach potentially interesting scientific goals, but they often have limited on-board power resources [1]. Monitoring robots inside industrial plants or rescue robots in disaster areas are occasionally disconnected from umbilical cables and can be difficult to reach by human operators [2]. Estimating driving energy in advance can be vital to their operational safety and to allow for coverage of longer distances.

In this work, we analyse the effect of unstructured geometries on driving energy consumption. While previous works have developed heuristic energy models that consider the terrain inclination as the main energy-relevant geometric factor [3] [4] [5] [6] [7], their prediction performance can decrease in highly uneven surfaces. For example, scattered rocks, steps, bumps and rough terrain can induce complex motion dynamics which pose a greater challenge to the robot locomotion and

control system, thereby leading to increased driving energy requirements. However, the complex interplay coming into action between wheel and terrain over unstructured geometries, and their effect on driving energy, can be challenging to model based on first principles. In this context, deep neural networks (DNNs) can be a well-suited asset, as they do not require explicit domain knowledge to be implemented into the prediction algorithm, and for their ability of extracting relevant features from high-dimensional data [8].

In this paper,

- We propose a DNN architecture to estimate the driving energy consumption and recovery of a mobile robot traversing unstructured terrains (Sections III-A and III-B). The main novelty of this paper is the use of a Convolutional 1D (Conv1D) neural network to analyse the 3D geometry of the terrain from perceived point cloud data. In our approach, point clouds are rearranged in the same temporal order as they would be experienced by the robot when traversing the terrain, and a Conv1D neural network is trained to capture the sequential context of the wheel-terrain interaction from which driving energy depends.
- The Conv1D neural network energy estimator is integrated into a lattice space A^* path planner (Section III-C). These two approaches are mutually beneficial to each other in that both energy estimation and path planning are achieved directly over feasible trajectories and unordered point clouds, thereby considering the actual traverse dynamic and the robot mobility constraints, and without any need of generating artificial 2D cost maps.
- The robustness of this method is demonstrated over data from several real unstructured scenarios (Section IV-A) and compared with a heuristic model which only considers the terrain inclination as geometric energy-relevant feature [3]. Particularly, we show that our model is robust to increasing levels of terrain roughness, while the latter substantially degrades its performance as the terrains deviate from planar (Sections V-A and V-B). Finally, we provide evidence of its benefit to reduce driving energy consumption (Section V-B).

To the best of the authors knowledge, this work is the first to propose an integrated energy-aware prediction and planning framework for mobile robots which considers the effect of complex unstructured terrain geometries.

II. RELATED WORK

Existing algorithms in the field of path planning in unstructured environments operate on a 2D-grid superimposed over the operational map [9] [10]. Each cell of the grid

Marco Visca and Saber Fallah are with the Connected and Autonomous Vehicles Lab (CAV Lab), University of Surrey, Guildford, GU2 7XH, UK. Email: {m.visca, s.fallah}@surrey.ac.uk

Arthur Bouton and Yang Gao are with the Space Technology for Autonomous and Robotic Laboratory (STAR LAB), Surrey Space Centre, University of Surrey, Guildford, GU2 7XH, UK. Email: {a.bouton, yang.gao}@surrey.ac.uk

Roger Powell is in the Cybernetics Group, Remote Applications in Challenging Environments, UK Atomic Energy Authority, Culham Science Centre, OX14 3DB.

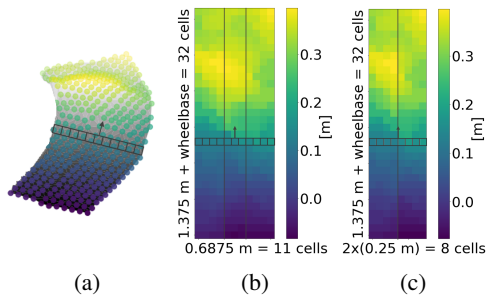


Fig. 1: Point Cloud data preprocessing pipeline. (a) Point cloud relative to trajectory is extracted from memory. (b) Point cloud is downsampled into a 2D voxel-grid. (c) The central region not in contact with the wheels is removed.

is assessed with specific traversability tests and, based on their results, assigned with a cost value. While this could be an effective and simple method to ensure reliable and safe navigation, expressing energy cost in this form can be challenging, as it assumes that each cell has a well defined intrinsic cost value. Besides, the cost functions used by grid methods are usually heuristic weighted combinations of terrain geometric properties such as slope, and roughness [11] [12] [13]. However, they do not provide an explicit estimation of energy consumption.

Other works have proposed the use of accurate onboard traverse simulators, which take as input geometric and other terrain information, and explicitly run a forward navigation simulation so as to assess the energy consumption of specific trajectories [13] [14] [15]. However, in spite of their accuracy, their computational workload is often excessive for real-time navigation, making them cumbersome to integrate into a path planning optimization framework.

Several machine learning techniques have been proposed to improve the path planning autonomy of mobile robots. This includes terrain classification [16] [17] [18], obstacle detection [19], slip prediction [20] [21], and terramechanical parameters estimation [22] [23] among the others. Specifically, artificial neural networks have gained an increasing popularity in this context for their ability to extract features from high-dimensional inputs, and their efficient parallel computing [8] [24]. Similarly to our work, Higa et al. [25] have proposed a deep learning method to estimate driving energy of a mobile robot on uneven terrains. Their implementation has the advantage to consider not only terrain geometry, but also its visual aspect by using a Convolutional 2D (Conv2D) neural network. However, in their work driving energy is correlated over squared patches of terrain. This can be considered as a static approximation, which associates an energy value to a terrain patch, but which does not capture the sequential context over the actual trajectory. Furthermore, they do not show how their method can be integrated into a path planner.

Different works have developed energy-aware path planners which explicitly estimates energy over feasible trajectories [3] [4] [5] [6]. However, they make use of heuristic energy models that only consider the terrain inclination as geometric energy-relevant feature. We argue that, while these approaches can be satisfactory for relatively planar

surfaces, they cannot capture the influence of more complex unstructured geometries. A similar implementation of the energy model developed in Gruning et al. [3], valid for our robotic platform, is used as main reference for qualitative and quantitative comparisons. We refer to it as RampModel in the rest of the paper. Furthermore, in their work two non-geometric factors are additionally considered for energy estimation: surface friction, and internal friction due to the track speed. However, as this work focuses on the effect of unstructured terrain geometries, surface friction and track speed are maintained constant during our experiments.

III. CONSTRUCTING THE ENERGY-AWARE PATH PLANNER

We propose to estimate driving energy end-to-end from point clouds by neural network training. Particularly, the neural network must be able to analyse the sequential context of the traversed terrain directly over feasible trajectories. In this way, driving energy estimation can be achieved by considering the actual traverse dynamics and the robot mobility constraints, thereby increasing the prediction accuracy. Moreover, the proposed approach allows to plan directly over unordered point clouds, without any need of cost map generation. This can be advantageous as point clouds can be easily obtained from any kind of range sensor, they are easy to maintain, and they can be split and merged with minimal computational effort [26]. The remainder of this section illustrates the proposed methodology.

A. Point Cloud Collection and Preprocessing

A diagram of the point cloud collection and preprocessing procedure is illustrated in Fig. 1. Points are retrieved from memory along the trajectory with a width equal to the wheel track (Fig. 1a). A safety check is performed before continuing with the preprocessing pipeline. The point cloud is analysed with standard geometric features extraction techniques to measure pitch, roll, and residual features [9]. If at least one of these values is above specific thresholds the trajectory is labelled as untraversable and is not considered for the energy planning optimisation. Conversely, if the point cloud passes the safety check, the preprocessing procedure can be continued. The point cloud is downsampled with a 2D-voxel grid having each of its row perpendicular to the local direction of the trajectory (Figs 1a and 1b). In this way, each row can be seen as the elevation points seen under a section of the rover along its width at a specific time, while each column represents the evolution of the terrain features under a specific location of the rover as it advances along the trajectory. Downsampling is motivated by the need of the neural network to have a fixed number of inputs to be used. Each cell of the voxel-grid is filled by averaging the elevation of all points in that cell, and by linear interpolation if no point is present. This choice does not introduce notable artefacts as long as the point cloud has a similar or higher density than the voxel discretization [27]. For our application, and in line with current on-board perception technologies [28], a uniform point cloud density of 256 pts/m² is assumed in a region up to 4 m distant from the robot. Next, the voxel discretization is set to a value of 6.25 cm × 6.25 cm.

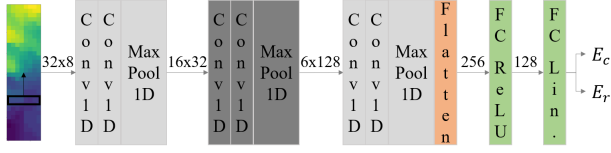


Fig. 2: Conv1D neural network architecture.

Finally, we can observe that all the elevation points in the central region of the voxel-grid have lower elevations than the rover belly, as they have passed the safety check. As a result, they do not interact with the robot and thereby do not impact the driving energy. Hence, only the two lateral bands, of width 25 cm each, are retained (Fig. 1c). The result of the point cloud preprocessing analysis is a 32×8 matrix of elevation values, which represents one input to the proposed neural network.

B. Neural Network Architecture

We propose to learn driving energy from point clouds by means of 1D convolutional neural network. Conv1D is a well known neural network architecture which has demonstrated remarkable performance in analysis of series of sensor data, signal processing and natural language processing [29]. Additionally, it has the advantage over alternative sequential methods (e.g. recurrent neural networks) to require lower training effort and to better exploit parallel computing [30]. Similarly, we propose to formulate our problem in a sequential fashion. Hence, Conv1D can be used to analyse the terrain sequence of Fig. 1c by means of a fixed-dimension 1D context window over the temporal (i.e. vertical) axis.

Fig. 2 shows the proposed Conv1D architecture. It consists of three stacks of two 1D convolutional layers followed by 1D max pooling. In this way, the bottom layers have the ability to learn a narrow temporal context, while wider temporal relationships can be learned at deeper layers. The first stack has kernel dimension $K = 2$ and zero padding, while the second and third stacks have $K = 3$ and no padding. The output of Conv1D is flattened and processed by one Fully Connected (FC) layer with 128 units and ReLU activation, followed by a FC layer with 2 units and linear activation. The outputs are the predicted energy consumption E_c and energy recovery E_r .

C. Planning Algorithm

Motion planning is performed in a state lattice space, a well known approach to the problem of differentially constrained mobile robot planning in unstructured environments [31]. State lattice is a search graph where vertices representing kinematic states of the robot are connected by edges representing trajectories that satisfy its kinematic constraints. In this way, planning and cost estimation can be achieved directly over feasible trajectories. In our application, we define a set of 9 elementary trajectories 1.375 m long, and with curvature uniformly spaced in $[-1.14, 1.14] \text{ m}^{-1}$, according to the mobility capability of our robot (see Fig. 3a).

The A* graph search optimisation is then used in the lattice space. This choice is motivated by the proven optimality of A* given a consistent heuristic [32], and by its simplicity and effectiveness to optimise paths according to complex cost

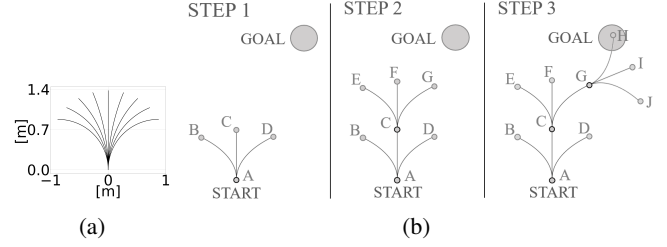


Fig. 3: (a) The 9 elementary trajectories of the lattice space, and (b) diagram of A* optimisation in lattice state space with only three actions for simplicity.

functions, making it well-suited to the robotic navigation in unstructured terrains [12]. Fig. 3b shows a diagram of the A* planning process for a lattice space with three actions. In the diagram, the start position is labelled as node A and added to a list called OPEN, which contains all nodes that have been found but not yet expanded. At each iteration of A*, a new node in the OPEN list is chosen according to its priority and expanded for the set of all elementary trajectories. In A* the priority is expressed as:

$$P(n) = C(n_p, n) + H(n, g) \quad (1)$$

The priority P of node n is given by the real cost $C(n_p, n)$ of moving from the parent node n_p to n , and the heuristic estimation $H(n, g)$ of the remaining cost from n to the goal g . The new node is then chosen as the one having the lowest P . The search continues until a goal node is retrieved from the OPEN list. At this point, by traversing backward the stored parent-child relationships, the path and the associated cost of A-C-G-H is found from the start to the goal. For more details on A* refer to [33].

In our application, $C(n_p, n)$ and $H(n, g)$ must have a meaning of driving energy. Particularly, the term $C(n_p, n)$ must represent the true value of energy when moving from state n_p to n . We propose a novel method to provide an estimate to this problem. For each new trajectory in the graph, the relative point cloud is retrieved from memory and preprocessed according to III-A and fed to the Conv1D neural network described in III-B. Its transition cost is then defined as: $C(n_p, n) = E_c - E_r$. On the contrary, the heuristic $H(n, g)$ does not require to provide the true energy value, but must be sufficiently informative to address the search algorithm in promising directions. The same $H(n, g)$ of the RampModel implementation is used, which assumes that the goal can be reached by moving on a straight line, and the heuristic for remaining energy is defined as:

$$H(n, g) = (G\theta + \beta)d \quad (2)$$

Where θ and d are respectively the relative inclination in degree and euclidean distance in meters between n and g , while G and β are heuristic parameters set to provide optimistic energy estimates. In this way, the consistency of the heuristic is guaranteed, thereby enabling the convergence of A* to an optimal solution. For our application, β is set to 1.90 J/m, while G is set to 6.13 J/m if θ is positive (i.e. uphill), and 1.18 J/m if θ is negative (i.e. downhill).

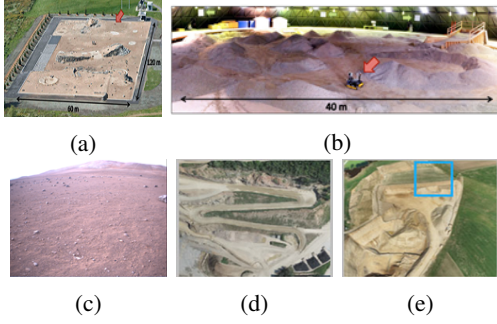


Fig. 4: Training dataset is (a) Canadian Space Agency (CSA) Martian Emulation Terrain (MET). Test datasets are (b) UTIAS indoor rover test facility, (c) Atacama desert SEEKER test trial, (d) mining quarry, and (e) gravel pit.

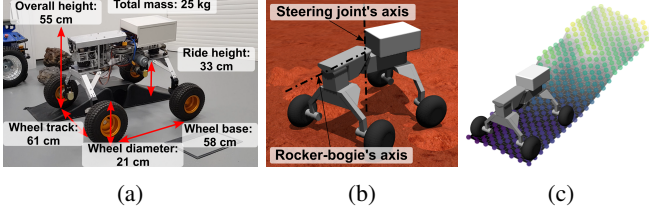


Fig. 5: (a) Features of the rover MARCEL. (b) Simulation model of the rover and its mobilities. (c) Example of the rover facing a trajectory sample to be analysed.

IV. EXPERIMENTAL SETUP

A. Simulation Environments

The algorithm is developed and tested using a physical simulator implemented in C++ and based on Open Dynamics Engine (ODE) [34] [35]. Different simulation environments are integrated in ODE from data collected from real uneven terrains (Fig. 4). Three of them are from Martian-like scenarios and collected using laser scans on-board wheel robotic platforms (Figs 4a, 4b and 4c). The other two are from a mining quarry and a gravel pit scenarios and collected with a fixed-wing flying robot using structure-from-motion techniques (Figs 4d and 4e). The datasets are all available online at [36] and [37] with the exception of the SEEKER dataset [38].

B. Robot Model

The numerical model of the robot is based on the features of the actual four-wheels rover prototype MARCEL first presented in [39] and depicted in Fig. 5. The rover is fitted with a rocker-bogie at the rear which ensures the contact of all wheels with the ground at all times. Indeed, this can be critical to guarantee consistent and energy-efficient driving over unstructured geometries. The rover is also provided with an actuated vertical pivot at the centre that allows it to steer smoothly. The wheels are synchronized with the steering joint rotation so that the rover can maneuver with theoretically no tangential and lateral skidding on a flat surface. The wheels are powered by four independent DC-motors subjected to PI speed controllers, while the steering joint has its own DC-motor and PID angular position controller. All the controllers run at a frequency of 1 kHz.

C. Ground Truth Energy Collection

This section illustrates how ground truth energy data are collected for training of the network described in Section III-B. The power of each motor is computed independently using the steady state equivalent circuit of the DC-motor armature [40]. The power of a DC motor is given by:

$$P = \frac{\omega\tau}{\eta} + R_a I_a^2 \quad (3)$$

The first term is the mechanical power, where ω is the motor angular speed, τ is the torque to the motor, and η is the motor efficiency due to mechanical losses. Mechanical power can be either consumed, if ω and τ have the same sign, and recovered, if they have opposite sign. The second term is the electrical power loss due to the motor resistance dissipated as heat, where R_a is the armature resistance and I_a is the current flowing into the motor. The current can also be expressed as follows:

$$I_a = \frac{\tau}{K_T g_r \eta} \quad (4)$$

Where, K_T is the motor torque constant, and g_r is the gear ratio. It follows that the power can be expressed as a function of ω and τ as:

$$P = \frac{\omega\tau}{\eta} + \left(\frac{\tau}{K_T g_r \eta} \right)^2 R_a \quad (5)$$

Simulated sensors on-board the robot measure ω and τ for each motor with a constant sampling rate Δt , and the power is computed with the formula in 5. Finally, assuming constant power between each Δt , the energy consumption E_c and the energy recovery E_r over the time interval $[t_0, t_f]$ can be computed as:

$$\begin{cases} E_c = \sum_{t_0}^{t_f} P_t \Delta t & P_t \geq 0 \\ E_r = \sum_{t_0}^{t_f} P_t \Delta t & P_t < 0 \end{cases} \quad (6)$$

For our platform, we assume: $\eta = 0.83$ if ω and τ have the same sign, and $\eta = 3.33$ if they have opposite sign, $R_a = 0.5 \Omega$, $K_T = 0.05 \text{ N} \cdot \text{m} \cdot \text{A}^{-1}$, $g_r = 62$, and $\Delta t = 10^{-3} \text{ s}$.

D. Training Dataset

We train the network by collecting data from the Canadian Space Agency (CSA) Martian Emulation Terrain (MET) (Fig. 4a), while we use the other environments for testing. The robot traverses the *MET* environment at constant speed of 20 cm/s and collects data from 107 606 trajectories, equivalent to approximately 150 km of traverse. The dataset is then randomly divided between training (80 %) and validation (20 %) datasets. Finally, the network is trained by means of stochastic gradient descent for 100 epochs (about 3 hours on a GeForce RTX 2080 Ti GPU) with mean squared error loss, 64 mini batch size, 10^{-4} learning rate, and RMSprop optimizer [41].

V. RESULTS

A. Test Results

The performance of Conv1D and RampModel are summarised in Table I. The first dataset, called *Ramps*, is a synthetic environment composed of perfectly planar ramps. The robot

TABLE I: Energy Estimation Test Results.

Dataset		Model	Consumption			Recovery			Total		
Name	Samples		MAE	MSE	R2	MAE	MSE	R2	MAE	MSE	R2
Ramps	1881	Conv1D	5.353	68.445	0.971	0.947	1.746	0.982	5.354	68.564	0.976
		RampModel	2.112	10.231	0.996	0.434	0.360	0.996	2.078	9.812	0.996
		Conv1D (25 %)	7.074	93.293	0.961	1.387	3.202	0.968	6.899	91.212	0.968
MET (val)	21578	Conv1D	4.804	65.526	0.939	0.568	0.654	0.983	4.549	60.792	0.956
		RampModel	14.182	385.477	0.640	1.169	2.743	0.930	13.343	342.075	0.750
		Conv1D (25 %)	5.505	78.255	0.927	0.687	0.906	0.977	5.181	72.217	0.947
SEEKER	33673	Conv1D	3.024	16.938	0.973	0.509	0.456	0.982	2.755	14.234	0.982
		RampModel	10.361	153.691	0.751	1.324	3.044	0.880	9.185	119.125	0.847
		Conv1D (25 %)	3.626	22.400	0.964	0.671	0.754	0.970	3.278	18.556	0.976
UTIAS	11668	Conv1D	6.656	98.209	0.906	1.010	1.910	0.903	6.172	89.859	0.919
		RampModel	21.969	717.477	0.315	2.843	11.393	0.421	19.423	588.190	0.469
		Conv1D (25 %)	7.599	120.944	0.885	1.327	3.341	0.830	6.885	105.803	0.904
Gravelpit	790	Conv1D	4.023	43.906	0.922	0.731	1.082	0.925	3.565	36.843	0.931
		RampModel	12.450	321.789	0.427	1.604	4.751	0.670	10.883	256.604	0.517
		Conv1D (25 %)	4.761	54.772	0.902	1.182	2.159	0.850	3.963	42.913	0.919
Quarry	4699	Conv1D	7.497	144.139	0.851	1.120	2.517	0.923	6.968	133.121	0.865
		RampModel	21.585	817.665	0.156	2.686	11.772	0.639	19.181	680.424	0.308
		Conv1D (25 %)	8.550	172.919	0.822	1.567	4.140	0.873	7.706	153.793	0.844

TABLE II: Path Planner Test Results.

Targets	Model	Planning Performance			Prediction Performance			Total Driving Energy	
		Nodes	Avg. Node Time [s]	Tot Time [s]	MSE	MAE	R2	Predicted [J]	Real [J]
259	Conv1D	5619	0.212	1265	271.938	7.882	0.937	16.268k	17.108k
	RampModel	2769	0.208	590	2514.917	33.724	0.269	9.368k	18.103k
	DynSim	3692	5.586	20699	0	0	1	15.623k	15.623k
1 (Fig. 6)	Conv1D	16	0.183	3.012	-	-	-	29.23	30.44
	RampModel	4	0.182	0.808	-	-	-	-0.99	39.33
	DynSim	12	4.324	51.750	-	-	-	27.72	27.72

traverses these ramps with 1881 trajectories having different combinations of pitch, roll and curvature. Conv1D has slightly lower performance than RampModel on *Ramps*. This can be explained by the fact that the former is a machine learning model which has been trained exclusively with data from unstructured environments, while the latter is a heuristic method ad-hoc devised for planar ramps. Nevertheless, both models retain satisfactory predictions, with Conv1D and RampModel total r2 score of 97.6 % and 99.6 % respectively. The results in the *Ramps* dataset show that RampModel accurately predicts driving energy in planar scenarios. However, we observe that its accuracy significantly degrades in unstructured surfaces, while Conv1D retains considerably better performance. Particularly, the RampModel total r2 score decreases to values of 30.8 % on *Quarry*, 46.9 % on *UTIAS*, 51.7 % on *Gravelpit*, 75.0 % on *MET*, and 84.7 % on *SEEKER*, while Conv1D is able to retain values of 86.5 %, 91.9 %, 93.1 %, 95.6 %, and 98.2 % respectively. We observe that the RampModel prediction of energy consumption is more largely affected than the energy recovery. A likely reason for this is that the energy recovery mostly depends on the downhill inclination of the terrain, making it less challenging, but still far from accurate, to estimate with RampModel. In contrast, the presence of steps, bumps, rough terrain and other complex geometries has a significant impact on the energy consumption, which can not be captured by an energy model exclusively based on terrain inclination. Conversely, Conv1D learns implicitly, by analysing the sequential context of the traversed terrain, the most relevant features to be correlated with driving energy and, in this way, retains better generalisation to the unforeseen un-

structured geometries. As a qualitative example, we analyse the terrain illustrated in Fig. 5c. It consists of an uphill trajectory with a series of scattered bumps. RampModel predicts a total driving energy of 54.99 J, which would be an accurate estimate for a planar terrain with the same inclination. However, the scattered bumps induce a greater energy demand on the robot actuators increasing the actual energy value to 108.29 J. As with previous results, this effect is more accurately captured by Conv1D, which predicts a total driving energy of 107.71 J.

We also test the performance of Conv1D when the training samples are reduced to 25 % of the original training dataset. A limited degradation of total r2 score can be observed with differences ranging from 0.6 % to 2.1 % depending on the test dataset. This shows evidence of the capability of Conv1D to retain similar performance with limited amount of data, which can be a crucial aspect in real-world applications.

B. Path Planner Integration Results

Conv1D and RampModel energy estimators are integrated into the A* lattice path planner. Their performance are assessed by conducting statistical analysis over 259 random start-goal positions within the different test environments. Table II summarises our findings. We observe that the number of nodes expanded by Conv1D is double that of RampModel. Specifically, over the 259 search problems Conv1D and RampModel expand respectively 5619 and 2769 nodes. A plausible explanation is that Conv1D has a larger disparity between the energy estimated by the heuristic $H(n, g)$ and the actual cost $C(n_p, n)$. An intrinsic property of the A* optimization is that the more optimistic the heuristic is compared to the

actual cost, the more A* has to expand the search. Therefore, Conv1D has to analyse a higher number of possible trajectories prior to find the optimal solution. While this results in longer planning time, Conv1D is nevertheless able to provide solutions which require lower driving energy consumption, and with considerably higher prediction accuracy. Specifically, the optimal predicted and real driving energy according to Conv1D is of respectively 16.268 kJ and 17.108 kJ, with a r2 score of 93.7 %. Conversely, RampModel provides a predicted solution of 9.368 kJ, but which has an actual energy demand of 18.103 kJ and a r2 score of 26.9 %. Therefore, Conv1D is able to provide solutions which consume 5.5 % less driving energy and to improve the r2 score prediction accuracy by 66.8 %. We also compare the two approaches with a ground truth method, called DynSim. In this method, the dynamic simulator, described in Section IV, is directly used to perform path planning. This means that the $C(n_p, n)$ values of each expanded node are measured by running the dynamic simulator and by measuring the driving energy with the method in IV-C. As this approach has access to the ground truth energy value during planning, it is able to provide exact predictions and the solution with the lowest driving energy, with a predicted and real energy value of 15.623 kJ. Therefore, the solution provided by Conv1D requires 9.5 % more driving energy than the ideal ground truth. However, DynSim assumes to have full domain knowledge of the environment during planning. While this is possible in the case of a simulator, it is often impractical in real-world scenarios. In contrast, Conv1D does not require any specific domain knowledge to be implemented, as it learns how to make energy estimations by collecting data. Hence, while in this paper we only focus on simulation, the Conv1D methodology can be in principle equally applicable to simulated and real-world scenarios. Moreover, the computational time of DynSim is measured to be more than 20 times higher than the other two methods. This provides insights on the often prohibitive computational workload of dynamic simulators for real-time planning. Specifically, we observe that, while Conv1D and RampModel have similar average node expansion times at around 0.2 s, DynSim takes on average 5.6 s. The three methods are tested on an Intel Core i9-9940X CPU and, for the feed forward computation of the neural network, on a GeForce RTX 2080 Ti GPU.

An example of the three different solutions according to the three energy estimation methods is given in Fig. 6, while their quantitative results are shown in the second part of Table II. As with the previous results, DynSim has an exact prediction accuracy, and provides the best solution with predicted and real energy values of 27.72 J. However, it also has the highest computational time with a total planning time of 51.8 s. In contrast, Conv1D provides a slightly more energy demanding solution with predicted and real energy value of respectively 29.23 J and 30.44 J, but in a fraction of the total planning time, with a value of 3.0 s. Moreover, the trajectory provided by Conv1D almost entirely corresponds to the one of DynSim. This provides evidence of the estimation accuracy of Conv1D, which results in a similar solution to the one selected by the ground truth method. Finally, RampModel has the shortest

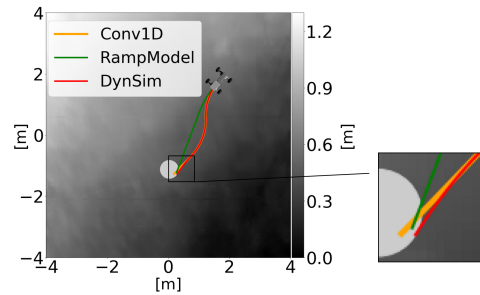


Fig. 6: Three different solutions to the A* optimisation with different energy estimation methods.

planning time, but also the lowest prediction accuracy, and the most energy demanding solution. We can interestingly observe how RampModel estimates its solution to provide a small quantity of energy recovery equal to -0.99 J. The robot proceeds on a slightly downhill trajectory and with a moderate roll inclination, which would lead to a marginal source of energy recovery if the surface was planar. However, the presence of unstructured geometries increases the actual energy to a value of 39.33 J. This confirms the higher robustness of our method which, by considering the actual terrain geometry, can provide more informed estimations and more energy efficient paths.

VI. CONCLUSION AND FUTURE WORKS

In this study, an integrated energy-aware prediction and planning framework is presented for mobile robots in unstructured environments. We remark the benefit of our methodology to (1) perform accurate driving energy estimations over unstructured terrain geometries by capturing the sequential context of the traversed terrain, and (2) reduce the robot driving energy by predicting and planning directly over feasible trajectories. We demonstrate the advantages of our methodology with respect to an inclination-based heuristic energy model to increase the prediction r2 score over planned trajectories by 66.8 % and reduce the driving energy consumption by 5.5 %. The considerable improvement of prediction accuracy is of particular relevance, as in many robotic applications an incorrect estimation of energy can compromise the safety and success of the mission.

We are extending this work in several directions. While in the current implementation trajectories were traversed at constant speed, the ability of our architecture to process data sequentially holds great promises for analysing the effect on driving energy of variable velocities. In addition, while this study analysed the effect on driving energy of terrain geometry, future works will consider strategies to include different terrain properties as an additional input to the proposed architecture. Finally, we intend to conduct experimental tests on a real robotic platform [39] to validate the results obtained during simulation.

ACKNOWLEDGEMENT

This work has been carried out within the framework of the EUROfusion Consortium and has received funding from the Euratom research and training programme under grant agreement No 633053. The views and opinions expressed herein do not necessarily reflect those of the European Commission. The authors are very grateful to the Autonomous Systems Group of RAL SPACE for providing the SEEKER dataset.

REFERENCES

- [1] O. Lamarre and J. Kelly, "Overcoming the challenges of solar rover autonomy: Enabling long-duration planetary navigation," *CoRR*, vol. abs/1805.05451, 2018.
- [2] E. Guizzo. Fukushima Robot Operator Writes Tell-All Blog. [Online]. Available: <https://spectrum.ieee.org/automaton/robotics/industrial-robots/fukushima-robot-operator-diaries>
- [3] V. Gruning, J. Pentzer, S. Brennan, and K. Reichard, "Energy-aware path planning for skid-steer robots operating on hilly terrain," in *2020 American Control Conference (ACC)*, 2020, pp. 2094–2099.
- [4] N. Ganganath, C. Cheng, and C. K. Tse, "A constraint-aware heuristic path planner for finding energy-efficient paths on uneven terrains," *IEEE Transactions on Industrial Informatics*, vol. 11, no. 3, pp. 601–611, 2015.
- [5] S. Fallah, B. Yue, O. Vahid-Araghi, and A. Khajepour, "Energy management of planetary rovers using a fast feature-based path planning and hardware-in-the-loop experiments," *IEEE Transactions on Vehicular Technology*, vol. 62, no. 6, pp. 2389–2401, 2013.
- [6] G. Sakayori and G. Ishigami, "Energy efficient slope traversability planning for mobile robot in loose soil," in *2017 IEEE International Conference on Mechatronics (ICM)*, 2017, pp. 99–104.
- [7] K. Otsu and T. Kubota, *Energy-Aware Terrain Analysis for Mobile Robot Exploration*. Cham: Springer International Publishing, 2016, pp. 373–388. [Online]. Available: https://doi.org/10.1007/978-3-319-27702-8_25
- [8] Y. LeCun, Y. Bengio, and G. Hinton, "Deep learning," *Nature*, vol. 521, no. 7553, pp. 436–444, 2015.
- [9] D. Sancho-Pradel and Y. Gao, "A survey on terrain assessment techniques for autonomous operation of planetary robots," *JBIS - Journal of the British Interplanetary Society*, vol. 63, no. 5-6, pp. 206 – 217, May 2010.
- [10] S. B. Goldberg, M. W. Maimone, and L. Matthies, "Stereo vision and rover navigation software for planetary exploration," in *Proceedings, IEEE Aerospace Conference*, vol. 5, March 2002, pp. 5–5.
- [11] J. Carsten, A. Rankin, D. Ferguson, and A. Stentz, "Global path planning on board the mars exploration rovers," in *2007 IEEE Aerospace Conference*, 2007, pp. 1–11.
- [12] M. Winter, C. Barclay, V. Pereira, R. Lancaster, M. Caceres, K. Mcmanamon, B. Nye, N. Silva, D. Lachat, and M. Campana, "Exomars rover vehicle: Detailed description of the gnc system," in *13th Symposium on Advanced Space Technologies in Robotics and Automation*, 05 2015.
- [13] G. Ishigami, K. Nagatani, and K. Yoshida, "Path planning and evaluation for planetary rovers based on dynamic mobility index," in *2011 IEEE/RSJ International Conference on Intelligent Robots and Systems*, 2011, pp. 601–606.
- [14] D. Helmick, A. Angelova, and L. Matthies, "Terrain adaptive navigation for planetary rovers," *Journal of Field Robotics*, vol. 26, 04 2009.
- [15] F. Zhou, R. E. Arvidson, K. Bennett, B. Trease, R. Lindemann, P. Bellutta, K. Iagnemma, and C. Senatore, "Simulations of mars rover traverses," *Journal of Field Robotics*, vol. 31, no. 1, pp. 141–160, 2014. [Online]. Available: <https://onlinelibrary.wiley.com/doi/abs/10.1002/rob.21483>
- [16] J.-F. Lalonde, N. Vandapel, D. Huber, and M. Hebert, "Natural terrain classification using three-dimensional lidar data for ground robot mobility," *J. Field Robotics*, vol. 23, pp. 839–861, 10 2006.
- [17] M. Ono, T. J. Fuchs, A. Steffy, M. Maimone, and J. Yen, "Risk-aware planetary rover operation: Autonomous terrain classification and path planning," in *2015 IEEE Aerospace Conference*, March 2015, pp. 1–10.
- [18] S. Zhou, J. Xi, M. McDaniel, T. Nishihata, P. Saleses, and K. Iagnemma, "Self-supervised learning to visually detect terrain surfaces for autonomous robots operating in forested terrain," *Journal of Field Robotics*, vol. 29, 03 2012.
- [19] C. Spiteri, A. Shaikat, and Y. Gao, "Structure augmented monocular saliency for planetary rovers," *Robotics and Autonomous Systems*, vol. 88, 11 2016.
- [20] R. Gonzalez and K. Iagnemma, "Slippage estimation and compensation for planetary exploration rovers. state of the art and future challenges," *Journal of Field Robotics*, vol. 35, no. 4, pp. 564–577, 2018.
- [21] R. González and K. Iagnemma, "Deepterramechanics: Terrain classification and slip estimation for ground robots via deep learning," *CoRR*, vol. abs/1806.07379, 2018. [Online]. Available: <http://arxiv.org/abs/1806.07379>
- [22] K. Iagnemma, Shinwoo Kang, H. Shibly, and S. Dubowsky, "Online terrain parameter estimation for wheeled mobile robots with application to planetary rovers," *IEEE Transactions on Robotics*, vol. 20, no. 5, pp. 921–927, Oct 2004.
- [23] K. Ho, T. Peynot, and S. Sukkarieh, "A near-to-far non-parametric learning approach for estimating traversability in deformable terrain," in *2013 IEEE/RSJ International Conference on Intelligent Robots and Systems*, Nov 2013, pp. 2827–2833.
- [24] P. Blacker, C. P. Bridges, and S. Hadfield, "Rapid prototyping of deep learning models on radiation hardened cpus," in *2019 NASA/ESA Conference on Adaptive Hardware and Systems (AHS)*, July 2019, pp. 25–32.
- [25] S. Higa, Y. Iwashita, K. Otsu, M. Ono, O. Lamarre, A. Didier, and M. Hoffmann, "Vision-based estimation of driving energy for planetary rovers using deep learning and terramechanics," *IEEE Robotics and Automation Letters*, vol. 4, no. 4, pp. 3876–3883, 2019.
- [26] P. Krüsi, P. Furgale, M. Bosse, and R. Siegwart, "Driving on point clouds: Motion planning, trajectory optimization, and terrain assessment in generic nonplanar environments," *Journal of Field Robotics*, vol. 34, no. 5, pp. 940–984, 2017. [Online]. Available: <https://onlinelibrary.wiley.com/doi/abs/10.1002/rob.21700>
- [27] C. Connolly, "Cumulative generation of octree models from range data," in *Proceedings. 1984 IEEE International Conference on Robotics and Automation*, vol. 1, 1984, pp. 25–32.
- [28] A. Shaikat, P. Blacker, C. Spiteri, and Y. Gao, "Towards camera-lidar fusion-based terrain modelling for planetary surfaces: Review and analysis," *Sensors*, vol. 16, no. 11, November 2016, (This article belongs to the Special Issue Vision-Based Sensors in Field Robotics). [Online]. Available: <http://epubs.surrey.ac.uk/812938/>
- [29] S. Kiranyaz, O. Avci, O. Abdeljaber, T. Ince, M. Gabbouj, and D. J. Inman, "1d convolutional neural networks and applications: A survey," *arXiv preprint arXiv:1905.03554*, 2019.
- [30] V. Peddinti, D. Povey, and S. Khudanpur, "A time delay neural network architecture for efficient modeling of long temporal contexts," in *Sixteenth Annual Conference of the International Speech Communication Association*, 2015.
- [31] M. Pivtoraiko, R. A. Knepper, and A. Kelly, "Differentially constrained mobile robot motion planning in state lattices," *Journal of Field Robotics*, vol. 26, no. 3, pp. 308–333, 2009.
- [32] R. Dechter and J. Pearl, "Generalized best-first search strategies and the optimality of A*," *J. ACM*, vol. 32, no. 3, p. 505–536, July 1985. [Online]. Available: <https://doi.org/10.1145/3828.3830>
- [33] P. E. Hart, N. J. Nilsson, and B. Raphael, "A formal basis for the heuristic determination of minimum cost paths," *IEEE Transactions on Systems Science and Cybernetics*, vol. 4, no. 2, pp. 100–107, July 1968.
- [34] A. Bouton, C. Grand, and F. Benamar, "Obstacle negotiation learning for a compliant wheel-on-leg robot," in *2017 IEEE International Conference on Robotics and Automation (ICRA)*, 2017, pp. 2420–2425.
- [35] —, "Motion control of a compliant wheel-leg robot for rough terrain crossing," in *2016 IEEE International Conference on Robotics and Automation (ICRA)*, 2016, pp. 2846–2851.
- [36] ASRL. ASRL - Autonomous Space Robotics Lab. [Online]. Available: <http://asrl.utias.utoronto.ca/>
- [37] senseFly. Elevation datasets. [Online]. Available: <https://www.sensefly.com/>
- [38] M. Woods, A. Shaw, E. Tidey, B. Van Pham, L. Simon, R. Mukherji, B. Maddison, G. Cross, A. Kisd, W. Tubby, G. Visentin, and G. Chong, "Seeker—autonomous long-range rover navigation for remote exploration," *Journal of Field Robotics*, vol. 31, no. 6, pp. 940–968, 2014.
- [39] A. Bouton and Y. Gao. MARCEL: A Mobile Active Rover Chassis for Enhanced Locomotion. [Online]. Available: <https://www.surrey.ac.uk/news/surrey-space-centre-wins-prestigious-robotics-award>
- [40] A. Sharma, N. Gupta, and E. Collins, "Energy efficient path planning for skid-steered autonomous ground vehicles," *Proceedings of SPIE - The International Society for Optical Engineering*, vol. 8045, 05 2011.
- [41] T. Tieleman and G. Hinton, "Lecture 6.5—RmsProp: Divide the gradient by a running average of its recent magnitude," COURSE: Neural Networks for Machine Learning, 2012.